Mimicking High-Silica Zeolites: Highly Stable Germanium- and Tin-Rich Zeolite-Type Chalcogenides

Qipu Lin,[†] Xianhui Bu,[*,‡] Chengyu Mao,[†] Xiang Zhao,[†] Koroush Sasan,[†] and Pingyun Feng[*,†]

[†]Department of Chemistry, University of California, Riverside, California 92521, United States

[‡]Department of Chemistry and Biochemistry, California State University, Long Beach, California 90840, United States

Ⓢ *Supporting Information*

ABSTRACT: High-silica zeolites, as exemplified by ZSM-5, with excellent chemical and thermal stability, have generated a revolution in industrial catalysis. In contrast, prior to this work, high-silica-zeolite-like chalcogenides based on germanium/tin remained unknown, even after decades of research. Here six crystalline high-germanium or high-tin zeolite-type sulfides and selenides with four different topologies are reported. Their unprecedented framework compositions give these materials much improved thermal and chemical stability with high surface area (Langmuir surface area of 782 m^2/g^{-1}) comparable to or better than zeolites. Among them, highly stable CPM-120-ZnGeS allows for ion exchange with diverse metal or complex cations, resulting in fine-tuning in porosity, fast ion conductivity, and photoelectric response. Being among the most porous crystalline chalcogenides, CPM-120-ZnGeS (exchanged with Cs^+ ions) also shows reversible adsorption with high capacity and affinity for CO_2 (98 and 73 cm^3 g^{-1} at 273 and 298 K, respectively, isosteric heat of adsorption = 40.05 kJ mol^{-1}). Moreover, CPM-120-ZnGeS could also function as a robust photocatalyst for water reduction to generate H_2. The overall activity of H_2 production from water, in the presence of $Na_2S-Na_2SO_3$ as a hole scavenger, was 200 μmol $h^{-1}/(0.10$ g). Such catalytic activity remained undiminished under illumination by UV light for as long as measured (200 h), demonstrating excellent resistance to photocorrosion even under intense UV radiation.

Crystalline porous materials (CPMs) lie at the center of many industrial applications including air separation and petroleum refining.[1] The rapid development of zeolites started in the late 1940s with the synthesis of low-silica (1 ≤ Si/Al ratio ≤ 1.5) zeolites such as zeolites A and X.[2] In the following decades, zeolites with various topologies and compositions were prepared. Among them, high-silica zeolites (Si/Al > 5) (e.g., ZSM-5),[3] known for their extraordinary stability, generated a revolution in industrial catalysis. Porous aluminophosphates were subsequently developed based on the analogy between SiO_2 and $AlPO_4$.[4] Since then, zeolite-type materials in other compositions (e.g., MOFs and zeolitic imidazolate frameworks, ZIFs) have also been developed.[5] ZIFs are actually analogs of all-silica (SiO_2) zeolites.

Compared to aforementioned insulating materials, porous chalcogenides are unique because of their intrinsic optoelec-tronic properties resulting from their narrow bandgaps, often in semiconducting range.[6] The pore size can also be much larger than zeolites, because of the larger building units in chalcogenides (e.g., supertetrahedral clusters).[7] Such integration between porosity and electronic and optical properties in chalcogenides make them highly promising for many applications.[6b,8]

One issue that has plagued practical applications of porous chalcogenides is stability. Clearly, the most straightforward strategy to enhance stability is to prepare Ge/Sn-rich high-silica-zeolite analogs. Unfortunately, decades of synthetic effects have yielded little or no success in this regard. At the beginning of such efforts in the late 1980s and early 1990s, it was found that Ge/Sn chalcogenides (without lower-valent metals) generally gave nonporous and low-dimensional structures.[9] A few open frameworks were made by using di- or monovalent ions (e.g., Mn^{2+}, Cu^+) as bridge to join together chalcogenide clusters (e.g., $Ge_4S_{10}{}^{4-}$).[10] Since the late 1990s, chalcogenide frameworks based on supertetrahedral clusters have become common, but they are generally dominated by trivalent ions such as In^{3+}, sometimes in combination with other metal ions such as Cu^+ and Cd^{2+}.[11] Prior to this work, chalcogenides most resembling zeolites are those based on M^{4+}/M^{3+} combinations discovered in the early 2000s.[12] But their M^{4+}/M^{3+} ratio (e.g., Ge^{4+}/Ga^{3+}, Sn^{4+}/In^{3+}) is unusually low (between 0.2 and 1.2), in most cases even lower than that in low-silica zeolites, in apparent violation of Löwenstein's rule (the Si/Al ratio ≥1 in zeolites).

It is therefore a major advance in the field of crystalline porous chalcogenides that in this study we have been able to realize Ge/Sn-rich chalcogenides with zeolite-type 4-connected porous frameworks, i.e., truly high-silica-zeolite-like in every aspect. Our success reported here resulted from the finding that a small amount of divalent metal ions could induce the crystallization of Ge/Sn chalcogenide zeotypes. This is an unusual discovery, because even in zeolites themselves, M^{4+}/M^{2+} combinations are extremely rare. VPI-7 and VPI-9 (zeolite type codes: VSV and VNI) based on zinc silicates are two exceptions.[13] Moreover, the family of Ge−S and Sn−Se materials reported here exhibit 4 different topologies (Table 1), illustrating the potential richness in this family of materials.

The availability of this family of high-silica-zeolite-like chalcogenides opens up access to many properties encompassing those that are generally reserved for insulting materials as well as those that are exclusively for semiconducting materials, from gas

Table 1. A Summary of Crystallographic Data of High-Ge/Sn Chalcogenide Zeolites[a]

code	F.C.	S.D.A.	topology	a [Å]	c [Å]	S.G.	R_1
1,CPM-120-ZnGeS	$Zn_{0.81}Ge_{3.19}S_8$	AEM	**sod-a**	20.7218	20.7218	$I\bar{4}3m$	0.081
2,CPM-121-ZnGeS	$Zn_{0.93}Ge_{3.07}S_8$	AEM/TBA	**dia-a**	11.2152	19.1197	$I\bar{4}2d$	0.048
3,CPM-122-ZnCdGeS	$Zn_{0.65}Cd_{0.41}Ge_{2.95}S_8$	AEM/2,6-Lutidine/DBU	**dia-a-a**	23.3607	39.2395	$I4_1/acd$	0.091
4,CPM-123-ZnGeS	$Zn_{1.21}Ge_{2.79}S_8$	AEM/HA	**crb-a**	21.5240	11.1160	$I\bar{4}$	0.057
5,CPM-120-ZnSnSe	$Zn_{0.99}Sn_{3.01}Se_8$	BPP	**sod-a**	22.4297	22.4297	$I\bar{4}3m$	0.061
6,CPM-120-CdSnSe	$Cd_{0.68}Sn_{3.32}Se_8$	BPP	**sod-a**	22.6140	22.6140	$I\bar{4}3m$	0.084

[a]F.C. = framework composition, S.D.A. = structure-directing agent, S.G. = space group, AEM = N-(2-aminoethyl)morpholine, TBA = tributylamine, DBU = 1,8-diazabicyclo[5.4.0]undec-7-ene, HA = 1-hexylamine, BPP = 1,3-bis(4-piperidinyl)propane. $R_1 = \sum ||F_{obs}| - |F_{calc}||/\sum|F_{obs}|$ (> 4.0 $\sigma(F)$).

sorption and ion exchange to photocatalysis and photoelectricity. Given half a dozen new phases reported here and various properties to be examined (see also Supporting Information (SI)), we chose CPM-120-ZnGeS (Table 1) as the representative to illustrate the broad range of properties made possible by our synthetic successes. These properties include gas separation of CO_2 over N_2 or CH_4, ion conductivity, photoelectric response, and photocatalytic activity for H_2 production from water.

As evidence for the greatly enhanced stability provided by our high-silica-mimicking method, CPM-120-ZnGeS was found in this work to show sustained high photocatalytic activity (200 μmol h^{-1}/(0.10 g)) for as long as measured (200 h under illumination of UV light) with a turnover number of >50. Moreover, such photocatalytic activity was achieved without any precious metal cocatalyst. Such resistance to photocorrosion is a very impressive achievement in the field of photocatalysis by chalcogenides.

In nonaqueous N-(2-aminoethyl)morpholine (AEM) solution, rhombic-dodecahedral crystals of CPM-120-ZnGeS were obtained in high yield (>95%) by solvothermal reaction of powder GeO_2, $Zn(NO_3)_2\cdot6H_2O$, and S. Its phase purity was confirmed by powder X-ray diffraction (XRD) and microscopic images. The formula of $[Zn_{0.81}Ge_{3.19}S_8]_n\cdot x$(amines) (amines are for protonated AEM and/or their decomposition fragments) was supported by single-crystal XRD, elemental analysis (EA, with C,H,N,S), thermogravimetric analysis (TGA), energy dispersive X-ray spectroscopy (EDX), and inductively coupled plasma mass spectrometry (ICP-MS). The detailed test data are provided in SI. By using different $M^{4+}/M^{2+}/X^{2-}$ (M^{4+} = Ge, Sn, M^{2+}=Zn, Cd, and X = S, Se) combinations and organic structure-directing agents, the framework compositions and topology types were broadened to include sulfides and selenides in 4 different topologies (synthesis procedure in SI). The crystallographic data and scanning electron microscopy (SEM) images for these high-Ge/Sn chalcogenides are given in Table 1 and Figure 1.

These high-silica-zeolite-like chalcogenides fall into 4 topologically distinct frameworks: augmented-sodalite (**sod-a**), augmented-diamond (**dia-a**), doubly augmented-diamond (**dia-a-a**), and augmented-CrB$_4$ (**crb-a**). With sodalite cages of ca. 18

Figure 2. (a) Supersodalite cage, and (b) tiling representation of 3D net of **1**. (c) Supertetrahedral T$_2$-cluster and (d) simple diamond (**dia**) net. (e) Augmented diamond (**dia-a**) net of **2** and (f) augmented-augmented diamond (**dia-a-a**) net of **3**. (g) Projection of structure of **4** and (h) augmented CrB$_4$ (**crb-a**) net.
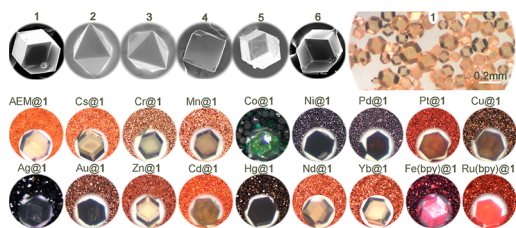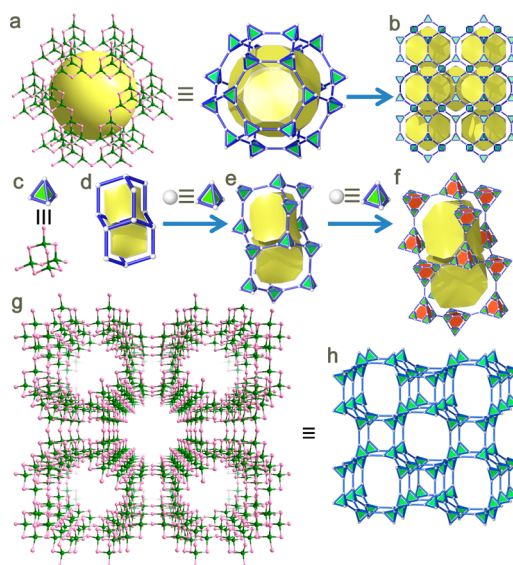

Figure 1. SEM images of chalcogenide zeolites (**1**−**6**) and photographs of **1** and its ion-exchanged variants M@**1**.

Å by diagonal distance, CPM-120 (Figure 2a,b) is built of corner-sharing supertetrahedral T$_2$ clusters into a 3D supersodalite (viz. **sod-a**) network, namely, zeolite-type **RWY** framework. As shown in Figure 2e−f, two diamond-like chalcogenide networks, with hierarchical augmentation, have been made in CPM-121 and −122, respectively. Also built of supertetrahedral T$_2$ cluster, the structure of CPM-121 could be simplified into a non-interpenetrated superdiamond (viz. **dia-a**) network. Interestingly, the framework of CPM-122 is further an augmented version of CPM-121, viz. **dia-a-a** net, in which the vertices of the **dia-a** net are replaced by T$_2$ clusters. The presence of adamantane-shaped T$_2$ clusters is also a key feature in CPM-123 (Figure 2g,h). The T$_2$ clusters are assembled into a tetragonal super CrB$_4$ (viz. **crb-a**) network with cylindrical channels of ca. 9 Å by diagonal distance. The "**crb**" notation is the same as zeolite framework type code **BCT**.

As calculated using the PLATON program, the solvent accessible volume of CPM-120-ZnGeS is 55%. TGA under nitrogen flow and powder XRD indicated that CPM-120-ZnGeS possesses high thermal stability up to ca. 610 °C. The sample also maintained structural and mechanical integrity when heated in air to at least 310 °C for 1 h (Figure 3a). The weight loss between 200 and 300 °C for AEM@**1** is related to the pyrolysis and loss of amine guests (Figure 3b). Powder XRD showed that CPM-120-ZnGeS is stable upon immersion in water or common solvents
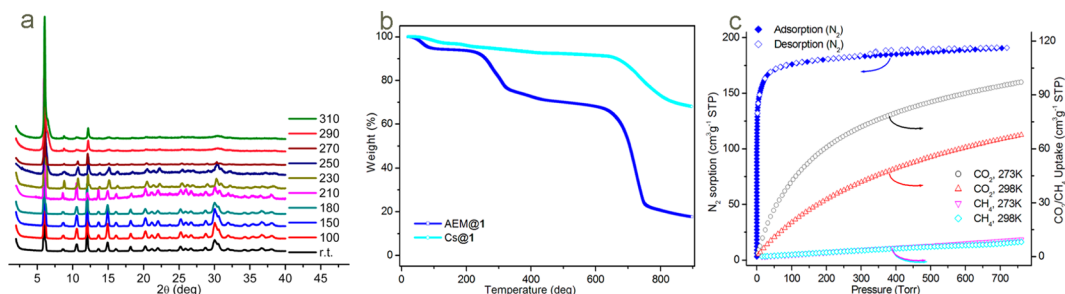
Figure 3. (a) Variable temperature PXRD and (b) TGA for **1**. (c) N_2 (77 K) and CO_2/CH_4 (273, 298 K) sorption isotherms for Cs@**1**.
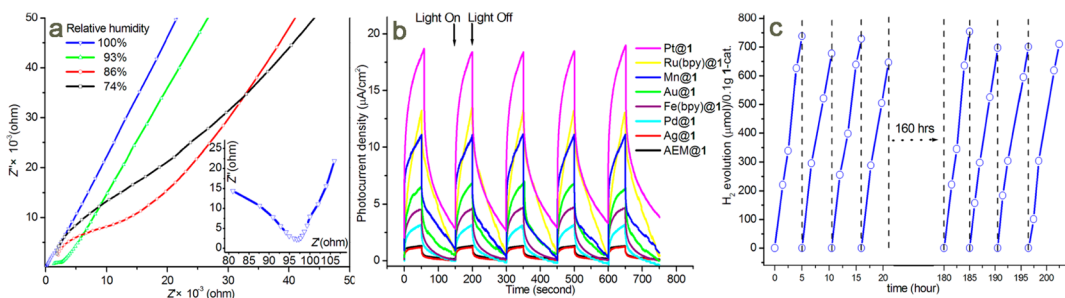
Figure 4. (a) Complex impedance plots under different relative humidity (RH) for Li@**1** (inset, enlarged for 100% RH). (b) Photoelectric response for the electrodes functionalized with **1** or ion-exchanged derivatives. The photocurrent density of Ag@**1** did not improve, due to its formation of Ag_2S phase. (c) Photocatalytic H_2 production over 0.10 g catalyst of **1** in 0.1 M Na_2SO_3 and 0.25 M Na_2S without loading cocatalysts.

such as acetone, acetonitrile, chloroform, tetrahydrofuran, methanol, and *N,N*-dimethylformamide for 24 h.

Ion-exchange was conducted using a range of metal salts or complex dyes to tune the porosity, fast ion conductivity, and band structure of CPM-120-ZnGeS (**1**). Typically, the freshly prepared crystals of **1** (also named AEM@**1**) were soaked in an aqueous (or acetonitrile) solution of metal salt (or complex) for 48 h, then taken out and washed with respective solvents to remove residual impurities on the surface. Photographs of **1** and its modified products M@**1** (M represents exchanged cation) are shown in Figure 1. The effectiveness of ion exchange was determined by EDX, ICP-MS, powder and single-crystal XRD, and optical spectra (e.g., solid-state UV−vis, photoluminescence). The detailed treatments and characterizations are provided in SI.

Due to the pore blockage by bulky organic templating agents, as-synthesized CPM-120-ZnGeS (AEM@**1**) showed negligible gas adsorption. Replacement of the protonated amines with alkali metal ions yielded much improved porosity. Among them, the Cs⁺-exchanged product (Cs@**1**) exhibited the type I isotherm with the Brunauer−Emmett−Teller (BET) and Langmuir surface areas of 599.16 and 781.78 m^2 g^{-1}, respectively (Figure 3c). It is worth noting that few crystalline chalcogenides exhibit porosity as confirmed by N_2 adsorption.[14] Further investigations on carbon capture were also performed. The CO_2 adsorption isotherms of Cs@**1** showed CO_2 uptake capacity of 98 and 73 cm^3 g^{-1} at 273 and 298 K, respectively, which to our knowledge is the best CO_2 adsorbing property among crystalline chalcogenides. In comparison, the isotherms of N_2/CH_4 at 273 and 298 K showed negligible uptake. These high selectivities of CO_2 over N_2/CH_4 can be attributed to the enhanced isosteric heat of adsorption (Q_{st}). Q_{st} for CO_2 adsorption was calculated using the Virial equation to be 40.05 kJ mol^{-1} at low coverage range (Figure S46), similar to that of Mg-MOF-74 with open metal sites.[15]

Compared to Cs@**1**, the lightest alkali metal ion, Li⁺, exchanged CPM-120-ZnGeS (viz. Li@**1**) showed much lower BET surface area of 90 m^2 g^{-1}, possibly due to much stronger aqua-complexation of Li⁺ ions and/or incomplete activation. On the other hand, among the NH_4^+, Li⁺, Na⁺, and Cs⁺ exchanged samples, Li@**1** displayed the highest ionic conductivity, reaching up to 1.62×10^{-3} S cm^{-1} at 24 °C. The ionic conductivities were assessed by AC impedance method using a compacted pellet (1.32 cm^2 × 0.2 cm). Under 100% relative humidity (RH), conductivity values obtained for other samples from the AC impedance plots are 2.05×10^{-4} S cm^{-1} (NH_4^+@**1**), 1.10×10^{-4} S cm^{-1} (Na@**1**) and 4.22×10^{-5} S cm^{-1} (Cs@**1**) (Figure S51). Among these, the Nyquist plot of Li@**1** exhibits a typical profile for low temperatures (<50 °C) with one semicircle and a linear tail at low frequencies (Figure 4a, inset). The weaker interactions between the chalcogenide framework and extra-framework charge carriers coupled with open channels could contribute to the material's high ionic conductivity. So far, most fast ion conductors show high performance at high temperatures (>100 °C).[16] Low temperature fast ion conductors are limited, but highly desirable.

The visible-light-driven photoelectric responses of postsynthetically modified variants of CPM-120-ZnGeS (M@**1**) have also been systematically studied here. By using a photo-electrochemical cell consisting of an F-doped SnO_2 (FTO) electrode coated with a thin layer of ground chalcogenide sample, a Pt-foil counter-electrode, and an Ag/AgCl reference electrode, the photogenerated electrons in M@**1** were collected by FTO substrates to generate anodic current. The photocurrent profiles (Figure 4b) show a rapid response and good reproducibility for all M@**1**'s electrodes in the on−off cycles of illumination. From the transient photocurrent plots, extra-framework precious metal cations or complex dyes led to significant differences. Among them, Pt@**1** electrode displayed the highest photocurrent density, which could be attributed to the rich photogenerated electron−hole pairs on the electrodes, revealing Pt's significant

role for charge transfer. The appearance of the anodic photocurrent suggests that all M@**1**'s films show typical n-type semiconductor behavior. Their enhanced conductivity, associated with the charge-transfer resistance under irradiation, was further confirmed by the electrochemical impedance spectroscopy (EIS) at low frequencies (Figure S56−63). From these results, it is clear that extra-framework compositions in **1** could induce a big difference in its photoelectric response behavior.

The robust framework, permanent porosity, and semiconducting properties make CPM-120-ZnGeS an excellent candidate for photocatalytic applications. The photocatalytic performance is often limited by the deactivation of the catalysts, especially the photocorrosion-prone metal sulfides. The H_2 evolution activity of CPM-120-ZnGeS was studied in a closed-gas circulation experiment, upon continuous irradiation with UV light (300 W xenon arc lamp) of degassed aqueous solutions containing $Na_2S-Na_2SO_3$ (as the sacrificial agent). The gas phase of the reaction was monitored by gas chromatography (GC) equipped with a thermal conductivity detector (TCD). This photocatalytic reaction exhibited a stable H_2 release rate of ca. 200 μmol h^{-1}/(0.1 g). Even after illumination of 200 h, the activity still remained with no noticeable decrease, demonstrating the excellent photostability of the sample. The turnover number (defined by the number of reacted electron to the number of atoms in a photocatalyst) was calculated to be >50. We have also examined the use of methanol as the hole scavenger instead of Na_2S and Na_2SO_3. The activity did not drop over the course of 24 h operation, again indicating its structural robustness and practical stability. The excellent photocatalytic performance and resistance to photocorrosion from UV radiation could be attributed to its Ge-rich high-silica-like composition.

In summary, six crystalline high-germanium or high-tin chalcogenide frameworks with four different topologies (i.e., supersodalite, superdiamond, supersuper-diamond, and superchromium tetraboride) are reported here. It has been demonstrated that multifunctional CPM-120-ZnGeS (**1**) is highly (thermally and chemically) stable, and allows for ion-exchange treatment to tune its porosity, ion conductivity, and photoelectric response. Exemplified by Cs$^+$-exchanged version, Cs@**1** exhibits high selectivity of CO_2 over CH_4 or N_2 at near room temperature. Importantly, supersodalite-like solid of **1** could be used as robust photocatalyst for water reduction to generate H_2. The overall activity of H_2 production from water, in the presence of $Na_2S-Na_2SO_3$ as a hole scavenger, was 200 μmol h^{-1}/(0.10 g). Such catalytic activity remains undiminished under illumination by UV light. The high content of Ge^{4+} species in the zeolitic chalcogenide CPM-120-ZnGeS contributes to its high thermal and chemical stability, which further dramatically improves its durability in the photocatalytic reaction. This work represents an important step toward the long-sought goal of building zeolitic chalcogenides with highly charged cations (i.e., Ge^{4+}, Sn^{4+}) that mimic the compositions of high-silica zeolites.

■ ASSOCIATED CONTENT

ⓢ Supporting Information

Experimental details, characterization data, crystallographic data (CIF files), and additional 3 tables and 75 figures. The Supporting Information is available free of charge on the ACS Publications website at DOI: 10.1021/jacs.5b03550.

■ AUTHOR INFORMATION

Corresponding Authors
*pingyun.feng@ucr.edu
*xianhui.bu@csulb.edu
Notes
The authors declare no competing financial interest.

■ REFERENCES

(1) (a) Flanigen, E. M.; Bennett, J. M.; Grose, R. W.; Cohen, J. P.; Patton, R. L.; Kirchner, R. M.; Smith, J. V. *Nature* **1978**, *271*, 512. (b) Feng, P. Y.; Bu, X. H.; Stucky, G. D. *Nature* **1997**, *388*, 735. (c) Li, H. L.; Laine, A.; O'Keeffe, M.; Yaghi, O. M. *Science* **1999**, *283*, 1145. (d) Corma, A.; Diaz-Cabanas, M. J.; Jorda, J. L.; Martinez, C.; Moliner, M. *Nature* **2006**, *443*, 842. (e) Corma, A.; Diaz-Cabanas, M.; Martinez-Triguero, J.; Rey, F.; Rius, J. *Nature* **2002**, *418*, 514.

(2) (a) Yu, J. H.; Xu, R. R. *Acc. Chem. Res.* **2010**, *43*, 1195. (b) Cheetham, A. K.; Ferey, G.; Loiseau, T. *Angew. Chem., Int. Ed.* **1999**, *38*, 3268.

(3) (a) Lermer, H.; Draeger, M.; Steffen, J.; Unger, K. K. *Zeolites* **1985**, *5*, 131. (b) Kokotailo, G. T.; Lawton, S. L.; Olson, D. H.; Olson, D. H.; Meier, W. M. *Nature* **1978**, *272*, 437.

(4) (a) Wilson, S. T.; Lok, B. M.; Messina, C. A.; Cannan, T. R.; Flanigen, E. M. *J. Am. Chem. Soc.* **1982**, *104*, 1146. (b) Bu, X. H.; Feng, P. Y.; Stucky, G. D. *Science* **1997**, *278*, 2080.

(5) (a) Park, K. S.; Ni, Z.; Cote, A. P.; Choi, J. Y.; Huang, R.; Uribe-Romo, F. J.; Chae, H. K.; O'Keeffe, M.; Yaghi, O. M. *Proc. Natl. Acad. Sci. U.S.A.* **2006**, *103*, 10186. (b) Phan, A.; Doonan, C. J.; Uribe-Romo, F. J.; Knobler, C. B.; O'Keeffe, M.; Yaghi, O. M. *Acc. Chem. Res.* **2010**, *43*, 58. (c) Zhang, H. X.; Liu, M.; Bu, X. H.; Zhang, J. *Sci. Rep.* **2014**, *4*, 3923. (d) Wang, F.; Fu, H. R.; Kang, Y.; Zhang, J. *Chem. Commun.* **2014**, *50*, 12065.

(6) (a) Dehnen, S.; Brandmayer, M. K. *J. Am. Chem. Soc.* **2003**, *125*, 6618. (b) Zheng, N.; Bu, X. H.; Vu, H.; Feng, P. Y. *Angew. Chem., Int. Ed.* **2005**, *44*, 5299.

(7) (a) Vaqueiro, P.; Romero, M. L.; Rowan, B. C.; Richards, B. S. *Chem.—Eur. J.* **2010**, *16*, 4462. (b) Vaqueiro, P.; Romero, M. L. *J. Am. Chem. Soc.* **2008**, *130*, 9630.

(8) Zheng, N. F.; Bu, X. H.; Feng, P. Y. *Nature* **2003**, *426*, 428.

(9) (a) Fard, Z. H.; Halvagar, M. R.; Dehnen, S. *J. Am. Chem. Soc.* **2010**, *132*, 2848. (b) Lin, Y. M.; Dehnen, S. *Inorg. Chem.* **2011**, *50*, 7913. (c) Lin, Y. M.; Massa, W.; Dehnen, S. *J. Am. Chem. Soc.* **2012**, *134*, 4497. (d) Xiong, W. W.; Miao, J. W.; Ye, K. Q.; Wang, Y.; Liu, B.; Zhang, Q. C. *Angew. Chem., Int. Ed.* **2015**, *54*, 546. (e) Liu, Y.; Kanhere, P. D.; Hoo, Y. S.; Ye, K. Q.; Yan, Q. Y.; Rawat, R. S.; Chen, Z.; Ma, J.; Zhang, Q. C. *RSC Adv.* **2012**, *2*, 6401.

(10) (a) Tan, K. M.; Darovsky, A.; Parise, J. B. *J. Am. Chem. Soc.* **1995**, *117*, 7039. (b) Haddadpour, S.; Melullis, M.; Staesche, H.; Mariappan, C. R.; Roling, B.; Clerac, R.; Dehnen, S. *Inorg. Chem.* **2009**, *48*, 1689. (c) Yaghi, O. M.; Sun, Z.; Richardson, D. A.; Groy, T. L. *J. Am. Chem. Soc.* **1994**, *116*, 807.

(11) (a) Su, W. P.; Huang, X. Y.; Li, J.; Fu, H. X. *J. Am. Chem. Soc.* **2002**, *124*, 12944. (b) Li, H. L.; Kim, J.; Groy, T. L.; O'Keeffe, M.; Yaghi, O. M. *J. Am. Chem. Soc.* **2001**, *123*, 4867. (c) Li, H. L.; Eddaoudi, M.; Laine, A.; O'Keeffe, M.; Yaghi, O. M. *J. Am. Chem. Soc.* **1999**, *121*, 6096.

(12) Zheng, N.; Bu, X.; Wang, B.; Feng, P. *Science* **2002**, *298*, 2366.

(13) (a) Rohrig, C.; Gies, H.; Marler, B. *Zeolites* **1994**, *14*, 498. (b) McCusker, L. B.; GrosseKunstleve, R. W.; Baerlocher, C.; Yoshikawa, M.; Davis, M. E. *Microporous Mater.* **1996**, *6*, 295.

(14) Feng, P. Y.; Bu, X. H.; Zheng, N. F. *Acc. Chem. Res.* **2005**, *38*, 293.

(15) Britt, D.; Furukawa, H.; Wang, B.; Glover, T. G.; Yaghi, O. M. *Proc. Natl. Acad. Sci. U.S.A.* **2009**, *106*, 20637.

(16) (a) Knauth, P. *Solid State Ionics* **2009**, *180*, 911. (b) Horike, S.; Umeyama, D.; Kitagawa, S. *Acc. Chem. Res.* **2013**, *46*, 2376.